

Progressive Open Space Expansion for Open-Set Model Attribution

Tianyun Yang¹², Danding Wang^{12*}, Fan Tang¹², Xinying Zhao¹², Juan Cao¹², Sheng Tang¹²

¹Institute of Computing Technology, Chinese Academy of Sciences, Beijing, China

²University of Chinese Academy of Sciences, Beijing, China

{yangtianyun19z, wangdanding, tangfan, zhaoxinying21s, caojuan, ts}@ict.ac.cn

Abstract

Despite the remarkable progress in generative technology, the Janus-faced issues of intellectual property protection and malicious content supervision have arisen. Efforts have been paid to manage synthetic images by attributing them to a set of potential source models. However, the closed-set classification setting limits the application in real-world scenarios for handling contents generated by arbitrary models. In this study, we focus on a challenging task, namely Open-Set Model Attribution (OSMA), to simultaneously attribute images to known models and identify those from unknown ones. Compared to existing open-set recognition (OSR) tasks focusing on semantic novelty, OSMA is more challenging as the distinction between images from known and unknown models may only lie in visually imperceptible traces. To this end, we propose a *Progressive Open Space Expansion (POSE)* solution, which simulates open-set samples that maintain the same semantics as closed-set samples but embedded with different imperceptible traces. Guided by a diversity constraint, the open space is simulated progressively by a set of lightweight augmentation models. We consider three real-world scenarios and construct an OSMA benchmark dataset, including unknown models trained with different random seeds, architectures, and datasets from known ones. Extensive experiments on the dataset demonstrate POSE is superior to both existing model attribution methods and off-the-shelf OSR methods. Github: <https://github.com/TianyunYoung/POSE>

1. Introduction

Advanced generative modeling technology can create extremely realistic visual content, leading to dramatic changes in the field of AI-enhanced design, arts, and metaverse [23, 41, 47]. Whereas, the broadcasting of malicious content generated by open source generation models has brought severe social impacts [9, 18, 43]. Furthermore,

*Corresponding author

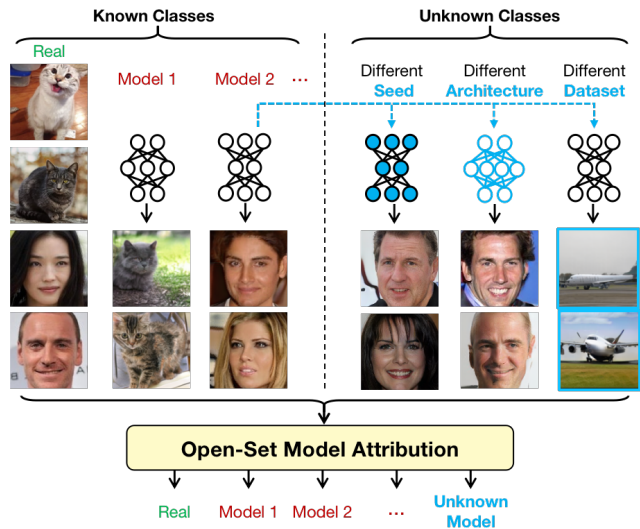


Figure 1. Open-set model attribution problem: The unknown classes include unknown models different from known models in training seeds, architectures, or training datasets. The goal is to simultaneously attribute images to known models and identify those from unknown ones.

new challenges have arisen for the ownership protection of copyrighted digital generative models. To solve these problems, model attribution, *i.e.*, identifying the source model of generated contents, has drawn increasing attention recently [5, 33, 48, 50, 53].

Marra *et al.* [33] are among the first to point out that GAN models leave specific fingerprints in the generated images, just like camera devices. Further researches [5, 14, 48, 50, 53] validate the existence of GAN fingerprints and show the feasibility of attributing fake images to a fixed and finite set of known models. However, most of these works focus on finding discriminative fingerprints among the contents generated by different GAN models following a simple closed-set setup. The ever-growing number of unseen source models in the real-world scenario appeal for a more generic approach. In this paper, we focus on the problem of Open-Set Model Attribution (OSMA), *i.e.*, simultaneously attributing images to known source models

and identifying those from unknown ones.

An intuitive way to solve OSMA is to apply off-the-shelf open-set recognition (OSR) approaches to closed-set model attribution classifiers. Traditional OSR methods leverage the output logits to either reject or categorize the input images [2, 44]. However, following the discriminative line, the performance highly depends on the closed-set classifier [46]. The learned feature space is not rectified for open-set samples. Another mainstream of OSR methods is based on simulating open-set samples or features [7, 27, 35, 36, 58]. By the simulation of open space, the learned feature space is more compact for closed-set categories [58], leading the detection of unknown samples more valid. Nevertheless, existing works only leverage a single generator [7, 27, 35] or mechanism [58] for simulating open-set samples or features, which are not diverse enough to reduce the open space risk for OSMA. A generator could produce open-set samples of different semantics, but its fingerprint is fixed and thus not suitable for the expansion of open space.

In this study, we propose *Progressive Open Space Expansion* (POSE) tailored for open-set model attribution, which simulates the potential open space of challenging unknown models through involving a set of augmentation models progressively. For augmentation model construction, it can be daunting to consider all types of unknown models with a variety of architectures. Instead, lightweight networks composed of a few convolution layers are employed. They serve as “virtual” follow-up blocks of known models, augmenting closed-set samples to open-set samples surrounding them by modifying their fingerprints with reconstruction residuals. Despite the simple structure, these augmentation models show the potential to model traces of a variety of unknown models. To enrich the simulated open space, multiple augmentation models are involved. Instead of training them independently, we design a progressive training mechanism to ensure the diversity of simulated open space across models in a computation-effective way.

To validate the effectiveness of POSE in the open world, we construct a benchmark dataset considering three challenging unknown scenarios as shown in Figure 1, which includes unknown models trained with either a different random seed, architecture or dataset from known models. Extensive experiments on the benchmark demonstrate POSE is superior to both existing GAN attribution methods and OSR methods. In summary, our contributions are:

- We tackle an important challenge for applying model attribution to open scenarios, the open-set model attribution problem, which attributes images to known models and identifies images from unknown ones.
- We propose a novel solution named POSE, which simulates the potential open space of unknown models progressively by a set of lightweight augmentation models, and consequently reduces open space risk.

- We construct an OSMA benchmark simulating the real-world scenarios, on which extensive experiments prove the superiority of POSE compared with existing GAN attribution methods and off-the-shelf OSR methods.

2. Related Work

Open-Set Recognition. Works on open-set recognition mainly follow a discriminative or generative line. The typical routine from the discriminative perspective first trains a K-way classifier on the closed set and then calibrates the confidence to a reasonable distribution for open-set discrimination [2, 44]. However, without rectification to the feature space, the performance depends heavily on the closed-set classifier [46]. Generative-based approaches employ generative models for two purposes: 1) to threshold the test-time reconstruction error as an open-set indicator [17, 38, 39, 45, 51, 57], or 2) to simulate the potential open space for augmenting classifier training [7, 8, 15, 27, 35, 36, 58]. For the open-set model attribution problem, it is sub-optimal to follow the reconstruction approach, as the intrinsic differences between samples generated by known and unknown models mainly lie in visually imperceptible traces, which are too subtle to be thresholded. For the second line, mixup mechanism [58], GAN [7, 27, 35], and auto-encoder [36] are leveraged for open space simulation. However, the open space risk for OSMA could be hardly reduced by a single generator or mechanism. The generators are proposed to generate images with different semantics, unable to produce diverse open-set fingerprints by its fixed weights and architecture. In this study, we simulate a rich open space for potential unknown models by involving a set of augmentation models progressively, and reduce the open space risk better.

Model Attribution. Model attribution aims to identify the source model of generated contents. Existing works tackle model attribution through an active [26, 54, 55] or passive manner [14, 16, 20, 33, 48, 49, 53]. Active methods embed artificial fingerprints [54, 55] or keys [26] into the generative model during the training process and then decouple them for source attribution in testing. Despite their capability of protecting particular models, requiring access to the training process limits their application in handling fake images generated by arbitrary models. With the verification of the existence of GAN fingerprints [33, 53], passive model attribution methods [14, 16, 20, 33, 48, 49, 53] are proposed by capturing the intrinsic differences in GAN fingerprints. Typically, a classifier is trained to distinguish images generated from a fixed and finite set of models, yet not applicable in the real world of an ever-growing number of unknown models. Some works, like DNA-Det [50] and RepMix [5], attempt to expand the application scenarios to identify images from unknown models of known architectures by relaxing the attribute objective to the model architecture

instead of a specific model. Though more generic compared with closed-set model attribution, architecture-level attribution still does not consider unknown models with unseen architectures. Girish *et al.* [16] pioneers to consider open-world GAN attribution and discovery. However, the proposed approach follows a general semi-supervised learning pipeline, overlooking the intrinsic challenge of imperceptible trace discrimination. Our proposed POSE is tailored for the trace discrimination challenge and achieves better performance in not only open-set model attribution but also unknown model clustering.

3. Method

We tackle the OSMA problem by simulating the potential open space of unknown models around the boundary of known space through a set of augmentation models. At a high level, for open space simulation, two key components are 1) the simulation tool, *i.e.*, how to construct the augmentation models, as it determines the scope of open space that could be expanded, and 2) the expansion mechanism. Given the augmentation models, the expansion mechanism decides how to increase the number of them to expand the open space in an efficient direction. In the following, we describe the simulation tool (Section 3.1) and expansion mechanism (Section 3.2) in detail.

3.1. Augmentation Model Construction

To simulate the space of unknown models, an intuitive way is to train a number of augmentation models approximating real unknown models. However, it is daunting to consider all types of unknown models of a variety of architectures. Empirically, we construct the augmentation models as lightweight networks by optimizing a reconstruction loss. Severing as “virtual” follow-up blocks of known models, augmentation models receive images from known models, maintain their semantics but modify the traces with reconstruction residuals. In this way, the augmented images would carry hybrid fingerprints of known classes and augmentation models as shown in Figure 3(b).

For the specific architecture choice, the candidate layer components could be upsampling and convolution. Upsampling layer would heavily influence high frequencies [6] and produce trivial open-set samples, which is thus not ideal to be included. As shown in [14], distinctions in GAN fingerprints exist in the frequency components. Equipped with rich learnable kernels, convolution layers are capable of modifying the frequencies, either suppressing or amplifying frequencies flexibly depending on the optimization objective [6]. Besides, [55] achieves GAN network fingerprinting by modulating convolution weights with a 128-bit fingerprint, reaching a capacity of around 10^{36} fingerprinted models in principle. Given these works suggesting the effect of convolution layers on GAN fingerprints, we use

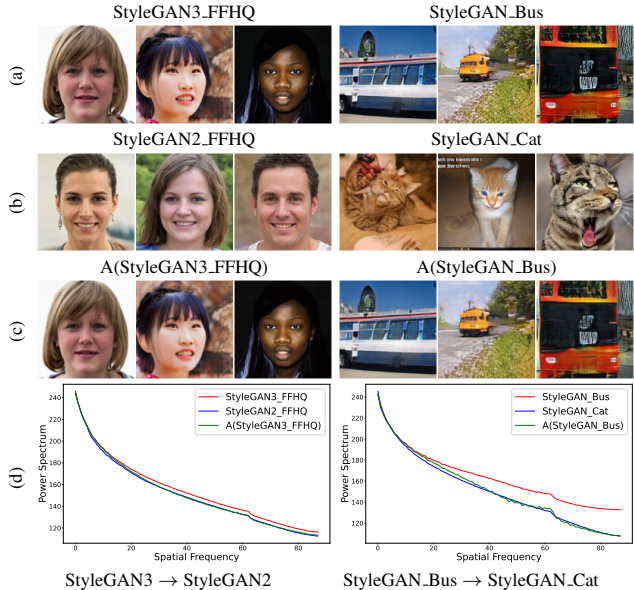


Figure 2. (a) Images generated by the source model M_1 . (b) Images generated by the respective target model M_2 . (c) Feed images from source model M_1 to an augmentation model A to simulate target model M_2 's trace while keeping the semantics unchanged. (d) Averaged azimuthal integral spectrum calculated on images from (a)-(c). X-axis means a specific radius on the 2D spectrum (or spatial frequency intuitively), and y-axis represents the sum of the spectrum magnitude of frequencies at this radius.

tiny networks with two convolution layers as augmentation models. Detailed ablation study is in Section 4.3.

Feasibility of tiny networks to simulate unknown model traces. It is non-trivial to measure the scope of open space that could be expanded. Motivated by existing work [14] showing that frequency spectrum contains much information about model fingerprints, we adopt a simple but characteristic 1D representation of the Fourier power spectrum, azimuthal integration (AI) over the power spectrum [13], as a hand-crafted criterion for the fingerprint space. Suppose M_1 is a known model and M_2 is a potential unknown model, to testify whether there exists an augmentation model A able to expand the open space around model M_1 to cover model M_2 according to the criterion, $\mathcal{L}_{\text{spectral}}$ is optimized as follows:

$$\mathcal{L}_{\text{spectral}}(\theta) = \|\mathbf{x} - A(\mathbf{x})\| + \lambda \|\text{Freq}(A(\mathbf{x}_1)) - \text{Freq}(\mathbf{x}_2)\|, \quad (1)$$

where θ is the parameters of A . \mathbf{x}_1 , \mathbf{x}_2 and \mathbf{x} are images generated by model M_1 , model M_2 , and all images. $\text{Freq}(\cdot)$ is spectrum azimuthal integration. λ is to balance two parts of $\mathcal{L}_{\text{spectral}}$. The first part is a pixel reconstruction loss constraining the reconstruction residual, and the second part is calculated in the frequency domain, converting the azimuthal integral spectrum of model A to model B .

As shown in Figure 2, by optimizing $\mathcal{L}_{\text{spectral}}$, augmentation models are able to transform the spectrum of

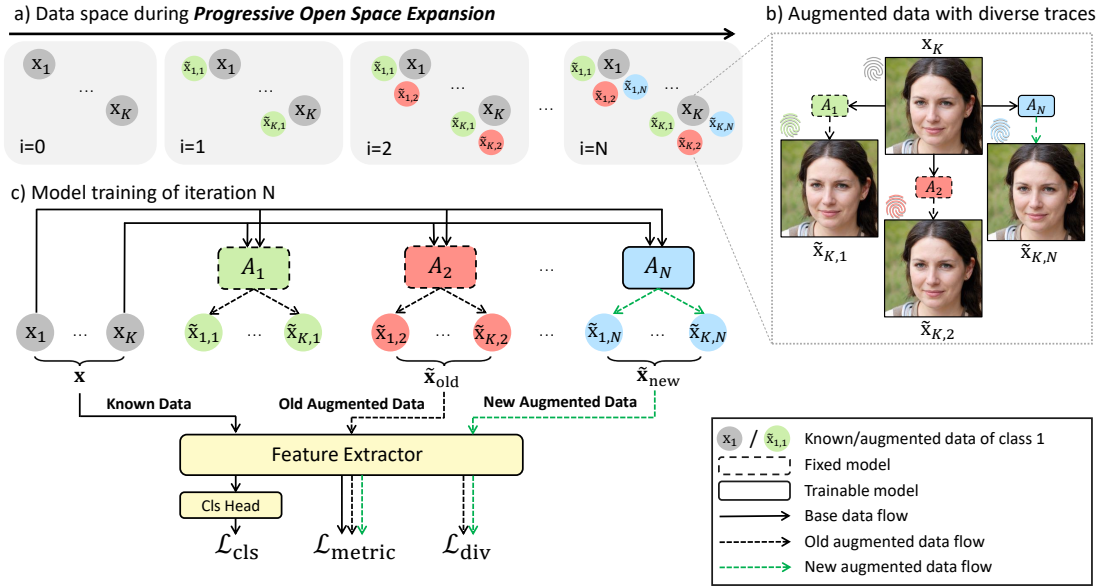


Figure 3. Overview of our proposed POSE. The open space is simulated by involving augmentation models progressively.

one model to another model of different architecture (e.g., StyleGAN3 \rightarrow StyleGAN2) or of different training dataset (e.g., StyleGAN_Bus \rightarrow StyleGAN_Cat) with visually imperceptible traces. These results suggest the potential of lightweight networks to simulate rich unknown traces. We also emphasize that unknown models are actually out of access in the real world. Our solution is to utilize a set of augmentation models to cover as much open space of potential unknown models as possible around the boundary of known space through a progressive training manner, which is described in Section 3.2.

3.2. Progressive Open Space Expansion

Figure 3 shows the framework of POSE. Our model consists of a task model and N augmentation models progressively involved. The task model M conducts open-set recognition task, including a feature extractor $F: \mathcal{X} \rightarrow \mathcal{Z}$ mapping images from the input space to the embedding space, and a classification head $H: \mathcal{Z} \rightarrow \mathcal{Y}$ for K -way known class classification, where K is the number of known classes. The augmentation models $\{A_i\}_0^{N-1}$ are trained progressively one at an epoch, simulating the open space by converting input images \mathbf{x} to augmented images $\tilde{\mathbf{x}}$.

Training augmentation models. Let $\tilde{\mathbf{x}}_{\text{new}}$ be the augmented images generated by the present augmentation model (with a solid edge), and $\tilde{\mathbf{x}}_{\text{old}}$ is generated by a randomly selected old augmentation model (with a dashed edge). The overall loss function for the present augmentation model is as follows:

$$\mathcal{L}_{\text{aug}} = \mathcal{L}_{\text{recons}}(\mathbf{x}, \tilde{\mathbf{x}}_{\text{new}}) + \mathcal{L}_{\text{div}}(\tilde{\mathbf{x}}_{\text{old}}, \tilde{\mathbf{x}}_{\text{new}}), \quad (2)$$

where $\mathcal{L}_{\text{recons}}$ is a reconstruction loss between augmented

and input images in the pixel space, and \mathcal{L}_{div} is a diversity constraint to enlarge the difference between new and old augmented data in the embedding space.

To expand the simulated open space, an intuitive way is to increase the number of augmentation models. However, naively increasing the number of augmentation models by training them independently could result in similar simulated open space across models as shown in Figure 5(top). Thus, we propose to increase the diversity progressively by constraining the discrepancy of old and new augmented data at each iteration. Simply increasing the embedding distance of $\tilde{\mathbf{x}}_{\text{new}}$ and $\tilde{\mathbf{x}}_{\text{old}}$ without direction would produce trivial samples also far from the known data. Hence, we apply a regularization term narrowing the embedding between new augmented images $\tilde{\mathbf{x}}_{\text{new}}$ and known images \mathbf{x} , to increase the diversity towards a direction approaching the known space:

$$\mathcal{L}_{\text{div}} = \alpha F_{\text{cos}}(\tilde{\mathbf{z}}_{\text{new}}, \tilde{\mathbf{z}}_{\text{old}}) - \beta \min(F_{\text{cos}}(\tilde{\mathbf{z}}_{\text{new}}, \mathbf{z}), d), \quad (3)$$

where F_{cos} refers to the cosine similarity loss. d is a distance margin to avoid the augmented data totally overlapping with known data. α and β are two hyper-parameters.

Training the task model. Given the known images \mathbf{x} , new and old augmented images $\tilde{\mathbf{x}}_{\text{old}}$ and $\tilde{\mathbf{x}}_{\text{new}}$. The overall loss function $\mathcal{L}_{\text{task}}$ for the task model is formulated as:

$$\mathcal{L}_{\text{task}} = \mathcal{L}_{\text{cls}}(\mathbf{x}) + \mathcal{L}_{\text{metric}}(\mathbf{x}, \tilde{\mathbf{x}}_{\text{old}}) + \mathcal{L}_{\text{metric}}(\mathbf{x}, \tilde{\mathbf{x}}_{\text{new}}), \quad (4)$$

where \mathcal{L}_{cls} is a cross-entropy loss for known class classification, and $\mathcal{L}_{\text{metric}}$ is a triplet loss to distinguish the embedding of augmented data from known data, and simultaneously

separating different known and augmented classes. $\mathcal{L}_{\text{metric}}$ is calculated on both new and old augmented data to avoid forgetting old open-set samples. Specifically, different from existing works taking all simulated open-set samples as a single $K + 1$ open class [36, 58], we assign different labels to augmented images from different known classes, as they carry diverse hybrid fingerprints. *e.g.*, for input images of class i and class j , we assign the augmented images by sending them into an augmentation model to different extended class labels $K + i$ and $K + j$. Then we sample triplets \mathcal{T} from the merged images of input and augmented data. $\mathcal{L}_{\text{metric}}$ is calculated on triplet sets as follows:

$$\mathcal{L}_{\text{metric}} = \sum_{\mathcal{T}_z \in \mathcal{T}} [\|x_a^z - x_p^z\|^2 - \|x_a^z - x_n^z\|^2 + m]_+, \quad (5)$$

where $\mathcal{T}_z = (x_a^z, x_p^z, x_n^z)$ is one triplet consisted of an anchor sample x_a^z , a positive sample x_p^z and a negative sample x_n^z . $[\cdot]_+ = \max(0, \cdot)$ denotes the hinge loss function. m is the violate margin that requires the distance of negative pairs to be larger than the distance of positive pairs, by at least a margin m . By optimizing $\mathcal{L}_{\text{metric}}$, known and augmented data are distinguished, and different known and augmented classes are separated simultaneously.

Training and Testing Procedure. The overall training progress is shown in Algorithm 1. In testing, the test image is fed into the feature extractor F and classification head H , getting predicted confidence scores for each class after a *softmax* function. In practice, if the max confidence score is larger than a threshold θ , the image is recognized as the known category corresponding to the index of the score. Otherwise, it is detected as unknown. We evaluate the overall closed/open discrimination performance by AUC and OSCR [12] calculated under diverse thresholds.

4. Experiments

4.1. Experimental Details

Datasets. We construct a benchmark for open-set model attribution in Table 1¹. There are four groups of data: Seen Real, Seen Fake, Unseen Real, and Unseen Fake², where Seen and Unseen mean whether images in this group are used for model attribution training or not. Detailed descriptions are as follows:

- **Seen Real:** Seven sets of real images: CelebA [31], Faces-HQ (1024 resolution face images containing CelebA-HQ [22] and FFHQ [24]), ImageNet [11], Youtube (real Youtube images from Faceforensics++ [42]), Bedroom, Cat and Bus images of LSUN [52].
- **Seen Fake:** Seen models trained on the seen real datasets

¹Here we only present one way to split this benchmark. The other four splits of the benchmark are in the supplementary material.

²We further include newly arisen stable-diffusion [41] models in the later stage of this work, results are shown in the supplementary material.

Algorithm 1 Progressive Open-Space Expansion (POSE)

Input: Known class images \mathbf{x} ; Number of epochs N

Output: Learned task model M ; Learned augmentation models $\{A_i\}_{i=0}^{N-1}$

- 1: **for** $i = 0, \dots, N$ **do**
 - 2: Generate augmented images $\tilde{\mathbf{x}}_{\text{new}}$ with $A_i(\mathbf{x})$
 - 3: **if** $i = 0$ **then**
 - 4: Train A_0 by $\mathcal{L}_{\text{recons}}(\mathbf{x}, \tilde{\mathbf{x}}_{\text{new}})$
 - 5: **else**
 - 6: Randomly select j from 0 to $i - 1$
 - 7: Generate augmented image $\tilde{\mathbf{x}}_{\text{old}}$ with $A_j(\mathbf{x})$
 - 8: Train A_i by $\mathcal{L}_{\text{recons}}(\mathbf{x}, \tilde{\mathbf{x}}_{\text{new}})$ and $\mathcal{L}_{\text{div}}(\tilde{\mathbf{x}}_{\text{old}}, \tilde{\mathbf{x}}_{\text{new}})$
 - 9: **end if**
 - 10: Train the task model M using $\mathcal{L}_{\text{task}}$
 - 11: **end for**
-

in the same columns. Each real dataset trains two models of different architectures.

- **Unseen Real:** Images from two real datasets non-overlapping with the seen reals, including CoCo [30] and Summer Yosemite images [59].

- **Unseen Fake:** Unseen models trained by partly the same settings with seen fake ones, but with different seeds, architectures, or training datasets. We control partly the same settings to consider the most challenging three scenarios. Please refer to Table 2 for the relationship between Seen and Unseen Fake. Three categories of Unseen Fake are:

- Unseen Seed: Unseen models of the same architecture and training data as certain seen fakes, but trained with different random seeds.
- Unseen Architecture: Unseen models trained on the same datasets as seen fakes, but with different architectures.
- Unseen Dataset: Unseen models of the same architecture as certain seen fakes, but trained on different datasets.

In total, the benchmark contains 15 known classes including real and 14 seen models, and 53 unknown classes including 10 unseen seed models, 22 unseen architecture models and 21 unseen dataset models. To be realistic, as shown in Table 3, in the testing set, Unseen Real are also considered as closed-set samples as it should be taken as the same known ‘real’ class as Seen Real, and Unseen Fake are taken as open-set classes. Compared with [16], our benchmark further considers two types of Unseen Fake (Unseen Seed and Unseen Dataset) and Unseen Real.

Evaluation. The performance is evaluated in two aspects: accurately classifying the known models, and distinguishing known and unknown models correctly, which are measured by accuracy and the area under ROC curve (AUC) respectively. We also report Open Set Classification Rate (OSCR) measuring the trade-off between the two aspects.

Implementation details. For the task model, the feature extractor includes a discrete cosine transform (DCT) trans-

Table 1. One split of the OSMA benchmark, including four groups: Seen Real, Seen Fake, Unseen Real, and Unseen Fake. Models in each column of Seen Fake, Unseen Seed, and Unseen Architecture are trained on the corresponding Seen Real dataset in the same column. Unseen Dataset include a total of 21 ProGAN, StyleGAN, and StyleGAN models trained on 7 datasets non-overlapping with Seen Real.

Seen Real	CelebA	Face-HQ	ImageNet	Youtube	LSUN-Bedroom	LSUN-Cat	LSUN-Bus
Seen Fake	StarGAN [10], ProGAN_seed0 [22]	StyleGAN3-r [23], StyleGAN3-t	SAGAN [56], SNGAN	FSGAN [37], FaceSwap [1]	ProGAN_seed0, MMDGAN	StyleGAN, StyleGAN3	ProGAN, StyleGAN
Unseen Seed	ProGAN (seed1,2,3,4,5)	-	-	-	ProGAN (seed1,2,3,4,5)	-	-
Unseen Fake	SNGAN [34], AttGAN [19], MMDGAN [3], InfoMaxGAN [28]	StyleGAN2 [25], ProGAN, StyleGAN [24]	S3GAN [32], BigGAN [4], ContraGAN [21]	Wav2Lip [40], FaceShifter [29]	SNGAN, InfoMaxGAN	SNGAN, ProGAN, MMDGAN, StyleGAN2	SNGAN, MMDGAN, StyleGAN2, StyleGAN3
Unseen Dataset	ProGAN, StyleGAN, StyleGAN3 (Cow, Sheep, Classroom, Bridge, Kitchen, Airplane, Church)						
Unseen Real	Coco, Summer						

Table 2. The relationship between Unseen Fake and Seen Fake.

Unseen Fake	Relationship with Seen Fake		
	Seed	Architecture	Dataset
Unseen Seed	Different	Same	Same
Unseen Architecture	-	Different	Same
Unseen Dataset	-	Same	Different

formation layer and a simple convolution network same as DNA-Det [50]. The reason for the DCT layer is that we find the distinctions of fingerprints in the frequency domain are more obvious than in the pixel domain. With the plain task model with by a cross-entropy loss, the closed-set accuracies are 90.67% and 83.53% for DCT and RGB input, while the AUCs on all unseen data are similar (73.78% and 74.26%). The classification head is an MLP network with two linear layers. The augmentation models have two convolution layers, whose weight shapes are $3 \times 32 \times 3 \times 3$ and $32 \times 3 \times 3 \times 3$, respectively. For optimization, we use the Adam optimizer with a step scheduler. The initial learning rate is set to 10^{-4} for task models and 10^{-2} for augmentation models. The hyper-parameter λ in $\mathcal{L}_{\text{spectral}}$ is set to 10^{-4} . For the hyper-parameters in \mathcal{L}_{div} , we empirically set $\alpha = 10^{-4}$, $\beta = 10^{-2}$, and $d = 0.95$. The violate margin m in $\mathcal{L}_{\text{metric}}$ is set to 0.3. Input images are all resized to 128px before sending into the network.

Compared methods. We compare against three groups of baselines: 1) GAN attribution, 2) GAN discovery and 3) open-set recognition methods. Most of them are not designed for the open-set model attribution problem. Compared methods and modifications to them are as follows:

- **GAN attribution:** PRNU [33], Yu *et al.* [53], DCT-CNN [14], DNA-Det [50], and RepMix [5]. We train them on the closed-set, and then obtain classification confidence scores on both the closed-set and open-set following the regular routine of OSR. Comparison results are in Table 4.

- **GAN discovery:** Girish *et al.* [16] focus on discovering newly arisen unseen GANs. To compare with this work, we

Table 3. Data split for training and testing process.

		Data Group
Train	Closed-Set	Seen Real, Seen Fake
Test	Closed-Set	Seen Real, Unseen Real, Seen Fake
	Open-Set	Unseen Fake

first train on the closed-set, and extract features for both the closed-set and open-set following the setup in [16], which are clustered by K-Means with the true cluster number and predicted cluster number by [16]. Results are in Table 5.

- **Open-set recognition:** The classical discriminative OSR method OpenMax [2] and three state-of-the-art generative OSR methods: PROSER [58], ARPL+CS [7], and DIAS [35]. Comparison results are in Table 6.

4.2. Evaluation of Open-Set Model Attribution

Comparison with GAN attribution methods. As shown in Table 4, POSE outperforms existing fake image attribution methods by a large margin in terms of AUC and OSCR. Specifically, the AUC points on unseen architecture, unseen dataset, and unseen all data are improved by 3.24%, 9.45%, and 11.02%, respectively, indicating the superiority of POSE in open-set discrimination. PRNU [33] achieves slightly higher AUC on seen seed, which may be because filters to extract PRNU noise are rather sensitive to differences in traces brought by model weights. We can also observe that unseen seed is the hardest open-set, unseen architecture the second, and unseen dataset is the easiest, which is consistent with our intuition as unseen seed and unseen architecture data only differ from seen data in visually imperceptible traces, and unseen seed data even shares the same model architecture. An exception case is DNA-Det [50], which performs well on unseen architecture, but poorly on unseen dataset. This is due to the fact that DNA-Det is designed to extract architecture traces regardless of the training dataset, yet data in unseen dataset

Table 4. Comparison with existing GAN attribution methods. Results are averaged among five splits of the benchmark.

Method	Closed-Set	Unseen Seed		Unseen Architecture		Unseen Dataset		Unseen All	
	Accuracy	AUC	OSCR	AUC	OSCR	AUC	OSCR	AUC	OSCR
PRNU [33]	55.27	69.20	49.16	70.02	49.49	67.68	48.57	68.94	49.06
Yu <i>et al.</i> [53]	85.71	53.14	50.99	69.04	64.17	<u>78.79</u>	72.20	69.90	64.86
DCT-CNN [14]	86.16	55.46	52.68	72.56	67.43	72.87	67.57	69.46	64.70
DNA-Det [50]	93.56	61.46	<u>59.34</u>	<u>80.93</u>	<u>76.45</u>	66.14	63.27	71.40	68.00
RepMix [5]	<u>93.69</u>	54.70	53.26	72.86	70.49	78.69	<u>76.02</u>	<u>71.74</u>	<u>69.43</u>
POSE	94.81	<u>68.15</u>	67.25	84.17	81.62	88.24	85.64	82.76	80.50

Table 5. Comparison with Girish *et al.* [16] for GAN discovery.

Method	Avg. Purity	NMI	ARI
Girish <i>et al.</i> [16] (k=49)	32.89	61.89	21.05
POSE (k=49)	39.16	61.91	27.48
POSE (k=68)	41.04	60.59	26.39

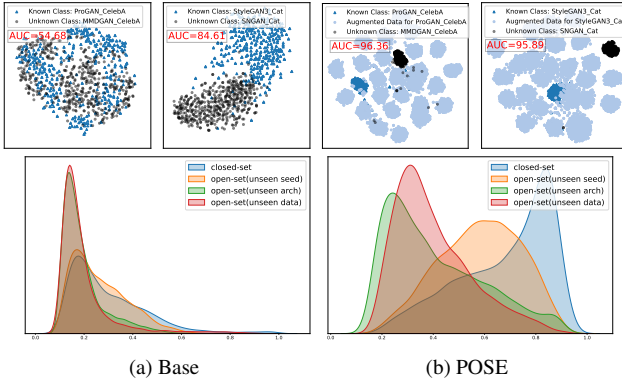


Figure 4. Feature space visualization (top) and confidence histograms (bottom) for Base method and our proposed POSE.

share the same model architectures as seen data.

Comparison with the GAN discovery method. To compare with Girish *et al.* [16] in discovering unseen models, we train POSE on seen data and obtain features for both the seen and unseen data, which are then clustered for two different values of cluster number k . $k = 68$ corresponds to the true number of classes for seen and unseen data. $k = 49$ represents the number of clusters that [16] returns after four iterations. Average purity, Normalized Mutual Information (NMI), and Adjusted Rand Index (ARI) are calculated to evaluate the clustering performance. Results are shown in Table 5. As seen, without iterative training on both seen and unseen data like [16], POSE is able to outperform in terms of purity and ARI, and get close NMI, which validates the efficiency of POSE in reasoning about unseen GAN classes.

Comparison with OSR methods. We take optimizing the plain task models by a cross-entropy loss as a Base method, and compare with OpenMax [2], PROSER [58], ARPL+CS [7], and DIAS [35] by employing their proposed techniques and simulated open-set samples to augment the

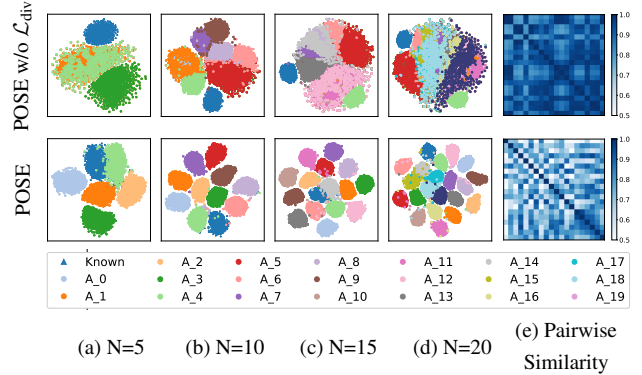


Figure 5. (a-d) Feature space visualization of progressive open space expansion process without (top) and with \mathcal{L}_{div} (bottom). Blue triangles are data of one known class, and circles in other colors are augmented data for this class by different augmentation models. (e) Pairwise similarities of open space expanded by 20 augmentation models. Bluer color indicates higher similarity.

Base classifier. As shown in Table 6, applying augmentation models (Base+AM) is superior to other OSR methods, and involving \mathcal{L}_{div} (Base+AM+ \mathcal{L}_{div}) gains further improvement. These results prove that the simulated open space by POSE is more suitable for OSMA than off-the-shelf OSR methods.

4.3. Ablation Study

Validation of training with augmentation models. As shown in Table 6, compared with the Base method, applying augmentation models (Base+AM) not only improves closed-set classification accuracy (from 90.68% to 93.41%) but also helps open-set discrimination (from 73.78% to 80.31% in AUC on unseen all data). This indicates simulating open space by augmentation models helps more compact feature extraction not only among close-set classes but also in between close/open-set. Meanwhile, observing the feature space visualization cases in Figure 4(top), the augmented data simulates a rich open space enclosing the known data points, resulting in a clear better close/open discrimination. Better open-set discrimination is also reflected in the prediction confidence scores in Figure 4(below), again justifying the effect of augmentation models.

Validation of \mathcal{L}_{div} . Figure 5(a-d) give an intuitive understanding of how \mathcal{L}_{div} influences the open space expansion

Table 6. Comparison with existing OSR methods and ablation experiments. Results are averaged among five splits of the benchmark.

Method	Closed-Set		Unseen Seed		Unseen Architecture		Unseen Dataset		Unseen All	
	Accuracy	AUC	OSCR	AUC	OSCR	AUC	OSCR	AUC	OSCR	
Base	90.68	62.02	60.58	76.03	72.92	77.01	73.88	73.78	70.97	
Base+OpenMax [2]	91.11	63.27	61.60	76.40	73.29	75.33	72.32	73.50	70.70	
Base+PROSER [58]	92.12	63.32	62.19	79.55	76.57	81.43	78.64	77.22	74.66	
Base+ARPL+CS [7]	91.77	54.94	54.17	79.09	75.97	80.48	77.52	75.08	72.47	
Base+DIAS [35]	92.77	62.15	61.02	79.34	76.49	84.14	81.13	78.00	75.41	
Base+AM	<u>93.41</u>	<u>66.17</u>	<u>65.04</u>	<u>82.21</u>	<u>79.42</u>	<u>85.04</u>	<u>82.20</u>	<u>80.31</u>	<u>77.80</u>	
Base+AM+ \mathcal{L}_{div} (POSE)	94.81	68.15	67.25	84.17	81.62	88.24	85.64	82.76	80.50	

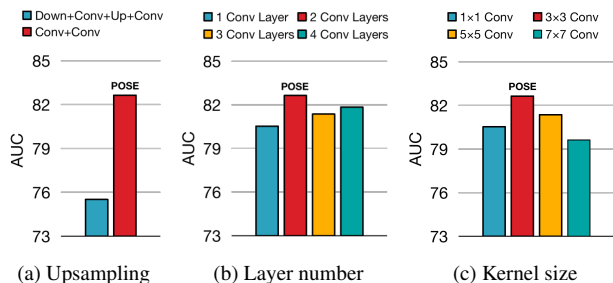


Figure 6. Ablation study on the architecture of augmentation models. We consider whether to include a upsample layer, layer number and kernel size of convolution layers.

progress. As seen, with \mathcal{L}_{div} added, the diversity of open space simulated by different augmentation models is largely increased, which is also indicated in the decreased pairwise similarity in Figure 5(e). Further, with the help of \mathcal{L}_{div} , the AUC points on unseen seed, architecture, dataset and unseen all data increase by 1.98%, 1.96%, 3.20%, and 2.45%. These results prove that employing \mathcal{L}_{div} increases the diversity of simulated open space and reduces the open space risk better.

Validation of the architecture of augmentation models.

We investigate the impact that the augmentation model’s architecture has on open-set discrimination performance from three aspects: 1) Upsampling layer. As discussed in Section 3.1, including upsampling in the augmentation model would heavily influence high frequencies and tend to produce trivial open-set samples. We empirically include upsampling layer in the augmentation model (Down+Conv+Up+Conv), resulting in much lower performance than two pure convolution layers (Conv+Conv) shown in Figure 6(a), which verifies our former assumption. 2) Layer number. In Figure 6(b), the AUC reaches the summit when the convolution layer number equals 2 and decreases with more layers. This may be due to that a single layer is hard to simulate large open space, while more layers lead to larger reconstruction residuals and produce easier open-set samples far from known space. 3) Kernel size. Figure 6(c) shows the AUC w.r.t. kernel size of convolution layers, indicating a 3×3 kernel size is the best. This could be because most generative models use a 3×3 kernel size.

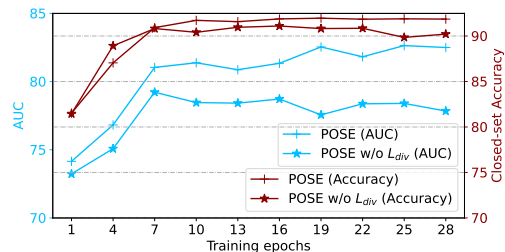


Figure 7. The influence of the number of augmentation models to open-set recognition performance.

Progressive vs. joint training. It is computation-expensive to jointly train a large number of augmentation models one-off and constrain the diversity among them. We compare the OSR performance of progressive and joint training with 9 augmentation models (the maximum number of augmentation models could be trained jointly on a 32G V100 GPU) on one split. At the 9th epoch with the same number of augmentation models involved, AUCs on unseen all data under progressive and joint training are 80.17% and 79.42%, while the latter takes five times longer to train than the former, which indicates progressive training provides an effective way to expand the open space.

Influence of the number of augmentation models. We study the effect of the number of augmentation models (N) in improving open-set recognition performance by plotting the AUCs and accuracies under different training epochs on one split in Figure 7. We can observe that the performance converges at early epochs without \mathcal{L}_{div} , while the AUC of POSE increases continually until about 19 epochs, indicating the necessity to increase the diversity of simulated open space.

5. Conclusions and Future Work

This paper tackles an important problem in applying model attribution to the real world, the open-set model attribution problem, to attribute images to known source models and identify those from unknown ones. We propose a novel progressive open space expansion solution for this problem, whose core idea is to simulate the potential open space of unknown models by involving augmentation mod-

els progressively. We consider three challenging types of unknown models to construct a benchmark simulating the real world attribution scenario. The superior experimental results indicate that it is promising to model the boundary of known models by artificially constructed models. In the future, it is fruitful to study how fingerprints are dominated by network components and simulate them by artificial tiny networks. This may result in better fingerprint space representation for more generic model attribution.

6. Acknowledgements

The research work is supported by the China Postdoctoral Science Foundation (2022TQ0344), the Project of Chinese Academy of Sciences (E141020), the National Natural Science Foundation of China (62203425), and the Zhejiang Provincial Key Research and Development Program of China (No.2021C01164).

References

- [1] Faceswap. <https://faceswap.dev>. 6, 13, 14
- [2] Abhijit Bendale and Terrance E Boult. Towards open set deep networks. In *CVPR*, 2016. 2, 6, 7, 8
- [3] Mikołaj Bińkowski, Dougal J. Sutherland, Michael Arbel, and Arthur Gretton. Demystifying MMD GANs. In *ICLR*, 2018. 6, 13, 14
- [4] Andrew Brock, Jeff Donahue, and Karen Simonyan. Large scale GAN training for high fidelity natural image synthesis. In *ICLR*, 2019. 6, 13, 14
- [5] Tu Bui, Ning Yu, and John Collomosse. Repmix: Representation mixing for robust attribution of synthesized images. In *ECCV*, 2022. 1, 2, 6, 7
- [6] Keshigeyan Chandrasegaran, Ngoc-Trung Tran, and Ngai-Man Cheung. A closer look at fourier spectrum discrepancies for cnn-generated images detection. In *CVPR*, 2021. 3
- [7] Guangyao Chen, Peixi Peng, Xiangqian Wang, and Yonghong Tian. Adversarial reciprocal points learning for open set recognition. *TPAMI*, 44(11):8065–8081, 2021. 2, 6, 7, 8
- [8] Guangyao Chen, Limeng Qiao, Yemin Shi, Peixi Peng, Jia Li, Tiejun Huang, Shiliang Pu, and Yonghong Tian. Learning open set network with discriminative reciprocal points. In *ECCV*, 2020. 2
- [9] Robert Chesney and Danielle Citron. Deepfakes and the new disinformation war: The coming age of post-truth geopolitics. Technical report, Foreign Aff., 2019. 1
- [10] Yunjey Choi, Minje Choi, Munyoung Kim, Jung-Woo Ha, Sunghun Kim, and Jaegul Choo. Stargan: Unified generative adversarial networks for multi-domain image-to-image translation. In *CVPR*, 2018. 6, 13, 14
- [11] Jia Deng, Wei Dong, Richard Socher, Li-Jia Li, Kai Li, and Li Fei-Fei. Imagenet: A large-scale hierarchical image database. In *CVPR*, 2009. 5
- [12] Akshay Raj Dhamija, Manuel Günther, and Terrance Boult. Reducing network agnostophobia. In *NeurIPS*, 2018. 5
- [13] Ricard Durall, Margret Keuper, and Janis Keuper. Watch your up-convolution: Cnn based generative deep neural networks are failing to reproduce spectral distributions. In *CVPR*, 2020. 3
- [14] Joel Frank, Thorsten Eisenhofer, Lea Schönherr, Asja Fischer, Dorothea Kolossa, and Thorsten Holz. Leveraging frequency analysis for deep fake image recognition. In *ICML*, 2020. 1, 2, 3, 6, 7
- [15] ZongYuan Ge, Sergey Demyanov, Zetao Chen, and Rahil Garnavi. Generative openmax for multi-class open set classification. In *BMVC*, 2017. 2
- [16] Sharath Girish, Saksham Suri, Sai Saketh Rambhatla, and Abhinav Shrivastava. Towards discovery and attribution of open-world gan generated images. In *ICCV*, 2021. 2, 3, 5, 6, 7
- [17] Yunrui Guo, Guglielmo Camporese, Wenjing Yang, Alessandro Sperduti, and Lamberto Ballan. Conditional variational capsule network for open set recognition. In *ICCV*, 2021. 2
- [18] Douglas Harris. Deepfakes: False pornography is here and the law cannot protect you. Technical report, Duke L. & Tech. Rev., 2018. 1
- [19] Zhenliang He, Wangmeng Zuo, Meina Kan, Shiguang Shan, and Xilin Chen. Attgan: Facial attribute editing by only changing what you want. *TIP*, 28(11):5464–5478, 2019. 6, 13, 14
- [20] Matthew Joslin and Shuang Hao. Attributing and detecting fake images generated by known gans. In *IEEE Security and Privacy Workshops*, 2020. 2
- [21] Minguk Kang and Jaesik Park. Contragan: Contrastive learning for conditional image generation. In *NeurIPS*, 2020. 6, 13, 14
- [22] Tero Karras, Timo Aila, Samuli Laine, and Jaakko Lehtinen. Progressive growing of gans for improved quality, stability, and variation. In *ICLR*, 2018. 5, 6, 13, 14
- [23] Tero Karras, Miika Aittala, Samuli Laine, Erik Härkönen, Janne Hellsten, Jaakko Lehtinen, and Timo Aila. Alias-free generative adversarial networks. In *NeurIPS*, 2021. 1, 6, 13, 14
- [24] Tero Karras, Samuli Laine, and Timo Aila. A style-based generator architecture for generative adversarial networks. In *CVPR*, 2019. 5, 6, 13, 14
- [25] Tero Karras, Samuli Laine, Miika Aittala, Janne Hellsten, Jaakko Lehtinen, and Timo Aila. Analyzing and improving the image quality of stylegan. In *CVPR*, 2020. 6, 13, 14
- [26] Changhoon Kim, Yi Ren, and Yezhou Yang. Decentralized attribution of generative models. In *ICLR*, 2021. 2
- [27] Shu Kong and Deva Ramanan. Opengan: Open-set recognition via open data generation. In *ICCV*, 2021. 2
- [28] Kwot Sin Lee, Ngoc-Trung Tran, and Ngai-Man Cheung. Infomax-gan: Improved adversarial image generation via information maximization and contrastive learning. In *WACV*, 2021. 6, 13, 14
- [29] Lingzhi Li, Jianmin Bao, Hao Yang, Dong Chen, and Fang Wen. Faceshifter: Towards high fidelity and occlusion aware face swapping. In *CVPR*, 2020. 6, 13, 14
- [30] Tsung-Yi Lin, Michael Maire, Serge Belongie, James Hays, Pietro Perona, Deva Ramanan, Piotr Dollár, and C Lawrence

- Zitnick. Microsoft coco: Common objects in context. In *ECCV*, 2014. 5, 11
- [31] Ziwei Liu, Ping Luo, Xiaogang Wang, and Xiaoou Tang. Deep learning face attributes in the wild. In *ICCV*, 2015. 5
- [32] Mario Lučić, Michael Tschannen, Marvin Ritter, Xiaohua Zhai, Olivier Bachem, and Sylvain Gelly. High-fidelity image generation with fewer labels. In *ICML*, 2019. 6, 13, 14
- [33] Francesco Marra, Diego Gragnaniello, Luisa Verdoliva, and Giovanni Poggi. Do gans leave artificial fingerprints? In *MIPR*, 2019. 1, 2, 6, 7
- [34] Takeru Miyato, Toshiki Kataoka, Masanori Koyama, and Yuichi Yoshida. Spectral normalization for generative adversarial networks. In *ICLR*, 2018. 6, 13, 14
- [35] WonJun Moon, Junho Park, Hyun Seok Seong, Cheol-Ho Cho, and Jae-Pil Heo. Difficulty-aware simulator for open set recognition. In *ECCV*, 2022. 2, 6, 7, 8
- [36] Lawrence Neal, Matthew Olson, Xiaoli Fern, Weng-Keen Wong, and Fuxin Li. Open set learning with counterfactual images. In *ECCV*, 2018. 2, 5
- [37] Yuval Nirkin, Yosi Keller, and Tal Hassner. Fsgan: Subject agnostic face swapping and reenactment. In *ICCV*, 2019. 6, 13, 14
- [38] Poojan Oza and Vishal M Patel. C2ae: Class conditioned auto-encoder for open-set recognition. In *CVPR*, 2019. 2
- [39] Pramuditha Perera, Vlad I Morariu, Rajiv Jain, Varun Manjunatha, Curtis Wigington, Vicente Ordonez, and Vishal M Patel. Generative-discriminative feature representations for open-set recognition. In *CVPR*, 2020. 2
- [40] KR Prajwal, Rudrabha Mukhopadhyay, Vinay P Namboodiri, and CV Jawahar. A lip sync expert is all you need for speech to lip generation in the wild. In *ACM MM*, 2020. 6, 13, 14
- [41] Robin Rombach, Andreas Blattmann, Dominik Lorenz, Patrick Esser, and Björn Ommer. High-resolution image synthesis with latent diffusion models. In *CVPR*, 2022. 1, 5, 11
- [42] Andreas Rössler, Davide Cozzolino, Luisa Verdoliva, Christian Riess, Justus Thies, and Matthias Nießner. FaceForensics++: Learning to detect manipulated facial images. In *ICCV*, 2019. 5
- [43] Raphael Satter. Experts: Spy used ai-generated face to connect with targets. Technical report, 2019. 1
- [44] Lei Shu, Hu Xu, and Bing Liu. Doc: Deep open classification of text documents. In *EMNLP*, 2017. 2
- [45] Xin Sun, Zhenning Yang, Chi Zhang, Keck-Voon Ling, and Guohao Peng. Conditional gaussian distribution learning for open set recognition. In *CVPR*, 2020. 2
- [46] Sagar Vaze, Kai Han, Andrea Vedaldi, and Andrew Zisserman. Open-set recognition: a good closed-set classifier is all you need? In *ICLR*, 2022. 2
- [47] Cong Wang, Fan Tang, Yong Zhang, Tieru Wu, and Weiming Dong. Towards harmonized regional style transfer and manipulation for facial images. *Computational Visual Media*, 9(2):351–366, 2023. 1
- [48] Xinsheng Xuan, Bo Peng, Wei Wang, and Jing Dong. Scalable fine-grained generated image classification based on deep metric learning. *arXiv preprint arXiv:1912.11082*, 2019. 1, 2
- [49] Tianyun Yang, Juan Cao, Qiang Sheng, Lei Li, Jiaqi Ji, Xirong Li, and Sheng Tang. Learning to disentangle gan fingerprint for fake image attribution. *arXiv preprint arXiv:2106.08749*, 2021. 2
- [50] Tianyun Yang, Ziyao Huang, Juan Cao, Lei Li, and Xirong Li. Deepfake network architecture attribution. In *AAAI*, 2022. 1, 2, 6, 7
- [51] Ryota Yoshihashi, Wen Shao, Rei Kawakami, Shaodi You, Makoto Iida, and Takeshi Naemura. Classification-reconstruction learning for open-set recognition. In *CVPR*, 2019. 2
- [52] Fisher Yu, Ari Seff, Yinda Zhang, Shuran Song, Thomas Funkhouser, and Jianxiong Xiao. Lsun: Construction of a large-scale image dataset using deep learning with humans in the loop. *arXiv preprint arXiv:1506.03365*, 2015. 5
- [53] Ning Yu, Larry S Davis, and Mario Fritz. Attributing fake images to gans: Learning and analyzing gan fingerprints. In *ICCV*, 2019. 1, 2, 6, 7
- [54] Ning Yu, Vladislav Skripniuk, Sahar Abdelnabi, and Mario Fritz. Artificial gan fingerprints: Rooting deepfake attribution in training data. In *ICCV*, 2021. 2
- [55] Ning Yu, Vladislav Skripniuk, Dingfan Chen, Larry Davis, and Mario Fritz. Responsible disclosure of generative models using scalable fingerprinting. In *ICLR*, 2022. 2, 3
- [56] Han Zhang, Ian Goodfellow, Dimitris Metaxas, and Augustus Odena. Self-attention generative adversarial networks. In *ICML*, 2019. 6, 13, 14
- [57] Hongjie Zhang, Ang Li, Jie Guo, and Yanwen Guo. Hybrid models for open set recognition. In *ECCV*, 2020. 2
- [58] Da-Wei Zhou, Han-Jia Ye, and De-Chuan Zhan. Learning placeholders for open-set recognition. In *CVPR*, 2021. 2, 5, 6, 7, 8
- [59] Jun-Yan Zhu, Taesung Park, Phillip Isola, and Alexei A Efros. Unpaired image-to-image translation using cycle-consistent adversarial networks. In *ICCV*, 2017. 5

The supplementary material is organized as follows:

- Section 7 provides the open-set discrimination result on images generated by a stable-diffusion model.
- Section 8 gives an analysis on two situations for open-set model attribution: unseen seed model and fine-tuned model.
- Section 9 gives robustness analysis against common image perturbations.
- Section 10 shows the full five splits of the OSMA benchmark.
- Section 11 visualizes randomly selected samples from the OSMA benchmark.

7. Evaluation on Diffusion Model

We evaluate samples generated by the newly arisen stable-diffusion model [41]. We use CoCo [30] captions to generate 1k stable-diffusion samples and test POSE’s open-set discrimination performance on these samples. Randomly selected samples are shown in Figure 10. As shown in Figure 8, the AUC point between closed-set and unseen stable-diffusion samples is 92.40, indicating that POSE is able to capture the difference in traces of known models and stable diffusion model, and recognize stable diffusion samples as from a new model.

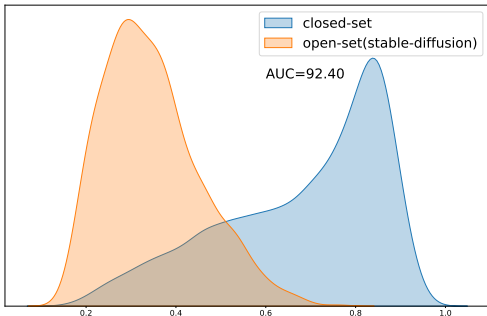


Figure 8. Confidence histograms on unseen stable diffusion data and closed-set data.

8. Unseen Seed and Finetuned Model

For open-set model attribution, there exist two situations near the known space boundary, *i.e.*, models trained with only seed different, and models fine-tuned from the known models. To analyze how POSE reacts in the two situations, we train a 2-way POSE classifier on {celeba, ProGAN_celeba_seed0}, and test the classifier on seven unseen models including ProGAN_celeba_seed1, and six models finetuned from ProGAN_celeba_seed0 on the celeba dataset. We plot in Figure 9 the confidence histograms for these models and calculate the weight distance between seen ProGAN_celeba_seed0 model and seven unseen models. Specifically, the weight distance between two models is

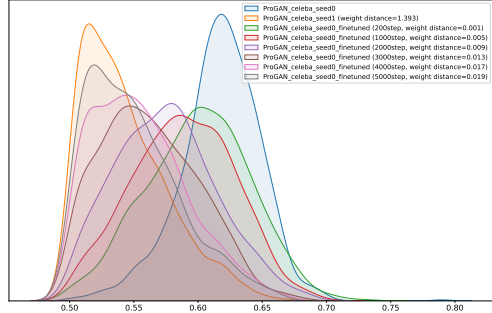


Figure 9. Confidence histograms on data from ProGAN_celeba_seed0, unseen seed model (ProGAN_celeba_seed1), and finetuned models (ProGAN_celeba_seed0_fineturned).

calculated as follows:

$$D(W_1, W_2) = \frac{1}{N} \sum_{i=1}^N \frac{\|W_{2,i} - W_{1,i}\|}{\|W_{1,i}\|}, \quad (6)$$

where W_1 and W_2 are weights of two models with the same architecture. N is the number of layers that are equipped with learnable weights.

As shown in Figure 9, the POSE classifier is able to separate samples generated by an unseen seed model (ProGAN_celeba_seed1) from seen ProGAN_celeba_seed0 model. With the finetune step increases (from 200 to 5000), the weight distance between the finetuned model and the original ProGAN_celeba_seed0 model increases followingly (from 0.001 to 0.019). When the weight distance reaches 0.019, POSE achieves a clear separation between the finetuned model and the original model. These results indicate that POSE is sensitive to trace changes brought by model weight changes, and is suitable for scenarios requiring strict attribution.

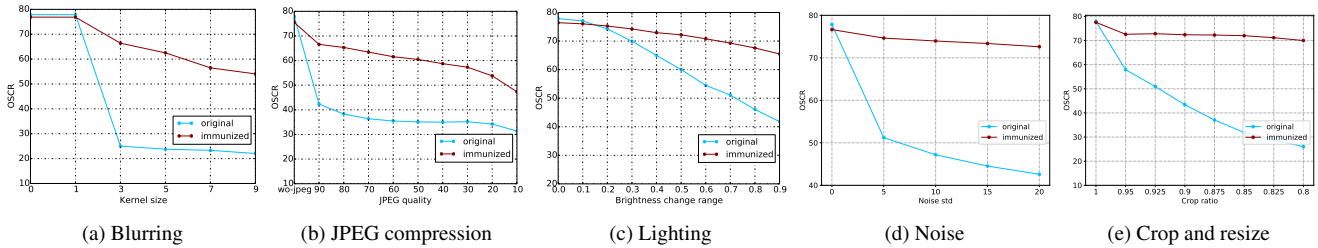
9. Robustness Analysis

Generated images may undergo post-processings in real-world scenarios. We evaluate the robustness of POSE against five common image perturbations, which are Blurring with Gaussian, JPEG compression, Lighting, additive Gaussian noise, crop, and resize. We evaluate the original version and immunized version of POSE. The original version indicates the perturbation is not included in model training, and the immunized version indicates that the perturbation is included as a kind of data augmentation in model training. We plot the OSCR results w.r.t the strength of each perturbation in Figure 11. As seen, without immunization, image perturbations would largely influence the model attribution performance. Nevertheless, with image perturbations included as data augmentation operations in model training, the performance drop is largely relieved. Specifically, the immunized version is rather robust to Lighting, Noise, and Crop perturbations. For



(a) A blue train in the middle of a forest. (b) A chain link fence contains a building and rubbish. (c) A clock sits high on a wall while below it on the wall features mosaic tiles. (d) A group of people in a field smile holding frisbees. (e) A soccer player trying to score a goal.

Figure 10. Randomly selected samples generated by the stable diffusion model.



(a) Blurring (b) JPEG compression (c) Lighting (d) Noise (e) Crop and resize

Figure 11. Robustness analysis. The results are evaluated on Split 1 of the benchmark.

JPEG compression quality $\sim [80, 100]$, and blur kernel size $\sim [0, 3]$, the performance drop could maintain within a 10% range.

10. Full Dataset Splits

We provide the full five splits of the OSMA benchmark in Table 7, Table 8, Table 9, Table 10, and Table 11, in which Table 7 is the same as Table 1 in the main text.

11. Visualization of Dataset Samples

We provide randomly selected samples in the benchmark for models trained on CelebA, Face-HQ, ImageNet, Youtube, LSUN-Bedroom, LSUN-Cat, and LSUN-Bus, which are shown in Figure 12.

Table 7. Split 1 of the OSMA benchmark.

Seen Real	CelebA	Face-HQ	ImageNet	Youtube	LSUN-Bedroom	LSUN-Cat	LSUN-Bus
Seen Fake	StarGAN [10], ProGAN_seed0 [22]	StyleGAN3-r [23], StyleGAN3-t	SAGAN [56], SNGAN	FSGAN [37], FaceSwap [1]	ProGAN_seed0, MMDGAN	StyleGAN, StyleGAN3	ProGAN, StyleGAN
Unseen Seed	ProGAN (seed1,2,3,4,5)	-	-	-	ProGAN (seed1,2,3,4,5)	-	-
Unseen Fake	SNGAN [34], AttGAN [19], MMDGAN [3], InfoMaxGAN [28]	StyleGAN2 [25], ProGAN, StyleGAN [24]	S3GAN [32], BigGAN [4], ContraGAN [21]	Wav2Lip [40], FaceShifter [29]	SNGAN, InfoMaxGAN	SNGAN, ProGAN, MMDGAN, StyleGAN2	SNGAN, MMDGAN, StyleGAN2, StyleGAN3
Unseen Dataset	ProGAN, StyleGAN, StyleGAN3 (Cow, Sheep, Classroom, Bridge, Kitchen, Airplane, Church)						
Unseen Real	Coco, Summer						

Table 8. Split 2 of the OSMA benchmark

Seen Real	CelebA	Face-HQ	ImageNet	Youtube	LSUN-Bedroom	LSUN-Cat	LSUN-Bus
Seen Fake	InfoMaxGAN [28], ProGAN_seed1 [22]	StyleGAN [24], StyleGAN3-t [23]	ContraGAN [21],	FSGAN [37], FaceShifter [29]	SNGAN, ProGAN_seed1	SNGAN, StyleGAN2	StyleGAN, StyleGAN3
Unseen Seed	ProGAN (seed0,2,3,4,5)	-	SNGAN -	-	ProGAN (seed0,2,3,4,5)	-	-
Unseen Fake	SNGAN [34], AttGAN [19], MMDGAN [3], StarGAN [10]	ProGAN, StyleGAN2 [25], StyleGAN3-r	S3GAN [32], BigGAN [4], SAGAN [56]	Wav2Lip [40], FaceSwap [1]	MMDGAN, InfoMaxGAN	ProGAN, MMDGAN, StyleGAN, StyleGAN3	ProGAN, SNGAN, MMDGAN, StyleGAN2
Unseen Dataset	SNGAN, StyleGAN, StyleGAN3 (Cow, Sheep, Classroom, Bridge, Kitchen, Airplane, Church)						
Unseen Real	Coco, Summer						

Table 9. Split 3 of the OSMA benchmark

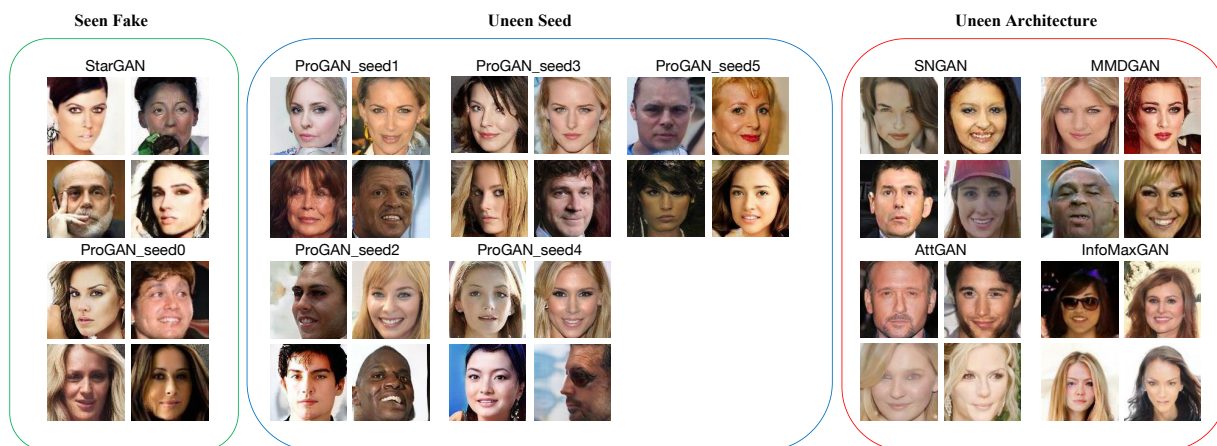
Seen Real	CelebA	Face-HQ	ImageNet	Youtube	LSUN-Bedroom	LSUN-Cat	LSUN-Bus
Seen Fake	AttGAN [19], ProGAN_seed2 [22]	ProGAN, StyleGAN3-t [23]	S3GAN [32], SNGAN	FaceSwap [1], FaceShifter [29]	InfoMaxGAN, ProGAN_seed2	SNGAN, ProGAN	ProGAN, MMDGAN
Unseen Seed	ProGAN (seed0,1,3,4,5)	-	-	-	ProGAN (seed0,1,3,4,5)	-	-
Unseen Fake	SNGAN [34], InfoMaxGAN [28], MMDGAN [3], StarGAN [10]	StyleGAN [24], StyleGAN2 [25], StyleGAN3-r	ContraGAN [21], BigGAN [4], SAGAN [56]	Wav2Lip [40], FSGAN [37]	MMDGAN, SNGAN	StyleGAN2, MMDGAN, StyleGAN, StyleGAN3	SNGAN, StyleGAN, StyleGAN3, StyleGAN2
Unseen Dataset	SNGAN, MMDGAN, ProGAN (Cow, Sheep, Classroom, Bridge, Kitchen, Airplane, Church)						
Unseen Real	Coco, Summer						

Table 10. Split 4 of the OSMA benchmark

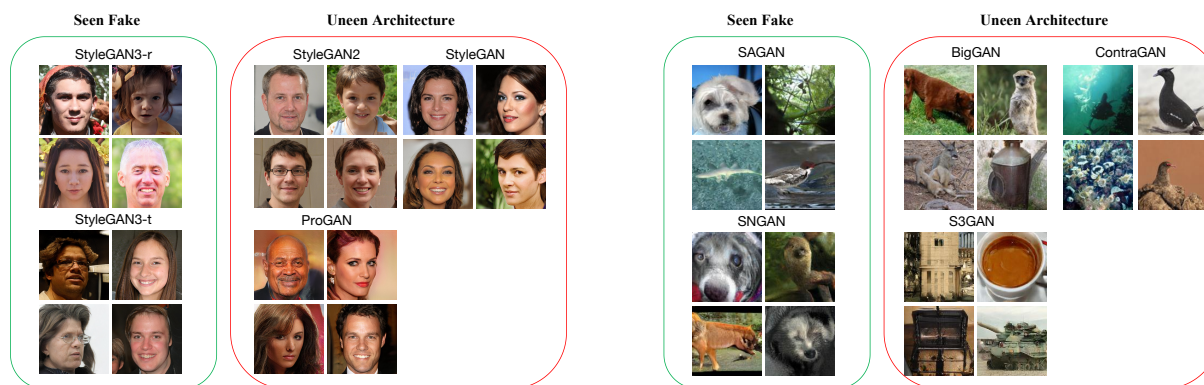
Seen Real	CelebA	Face-HQ	ImageNet	Youtube	LSUN-Bedroom	LSUN-Cat	LSUN-Bus	
Seen Fake	SNGAN [34], ProGAN_seed3 [22]	ProGAN, StyleGAN3-r [23]	ContraGAN [21],	Wav2Lip [40], FSGAN [37]	SNGAN, ProGAN_seed3	ProGAN, MMDGAN	SNGAN, MMDGAN	
Unseen Fake	Unseen Seed	ProGAN (seed0,1,2,4,5)	-	BigGAN [4]	-	ProGAN (seed0,1,2,4,5)	-	
	Unseen Architecture	AttGAN [19], InfoMaxGAN [28], MMDGAN [3], StarGAN [10]	StyleGAN [24], StyleGAN2 [25], StyleGAN3-t	S3GAN [32], SNGAN, SAGAN [56]	FaceSwap [1], FaceShifter [29]	MMDGAN, InfoMaxGAN	SNGAN, StyleGAN, StyleGAN2, StyleGAN3	ProGAN, StyleGAN, StyleGAN2, StyleGAN3
	Unseen Dataset	SNGAN, ProGAN, MMDGAN (Cow, Sheep, Classroom, Bridge, Kitchen, Airplane, Church)						
Unseen Real	Coco, Summer							

Table 11. Split 5 of the OSMA benchmark

Seen Real	CelebA	Face-HQ	ImageNet	Youtube	LSUN-Bedroom	LSUN-Cat	LSUN-Bus	
Seen Fake	AttGAN [19], ProGAN_seed4 [22]	StyleGAN [24], StyleGAN3-t [23]	ContraGAN [21],	FaceSwap [1], Wav2Lip [40]	InfoMaxGAN, ProGAN_seed4	StyleGAN, ProGAN	ProGAN, MMDGAN	
Unseen Fake	Unseen Seed	ProGAN (seed0,1,2,3,5)	-	BigGAN [4]	-	ProGAN (seed0,1,2,3,5)	-	
	Unseen Architecture	SNGAN [34], InfoMaxGAN [28], MMDGAN [3], StarGAN [10]	ProGAN, StyleGAN2 [25], StyleGAN3-r	S3GAN [32], SNGAN, SAGAN [56]	FaceShifter [29], FSGAN [37]	MMDGAN, SNGAN	StyleGAN2, MMDGAN, SNGAN, StyleGAN3	SNGAN, StyleGAN, StyleGAN3, StyleGAN2
	Unseen Dataset	ProGAN, MMDGAN, StyleGAN (Cow, Sheep, Classroom, Bridge, Kitchen, Airplane, Church)						
Unseen Real	Coco, Summer							

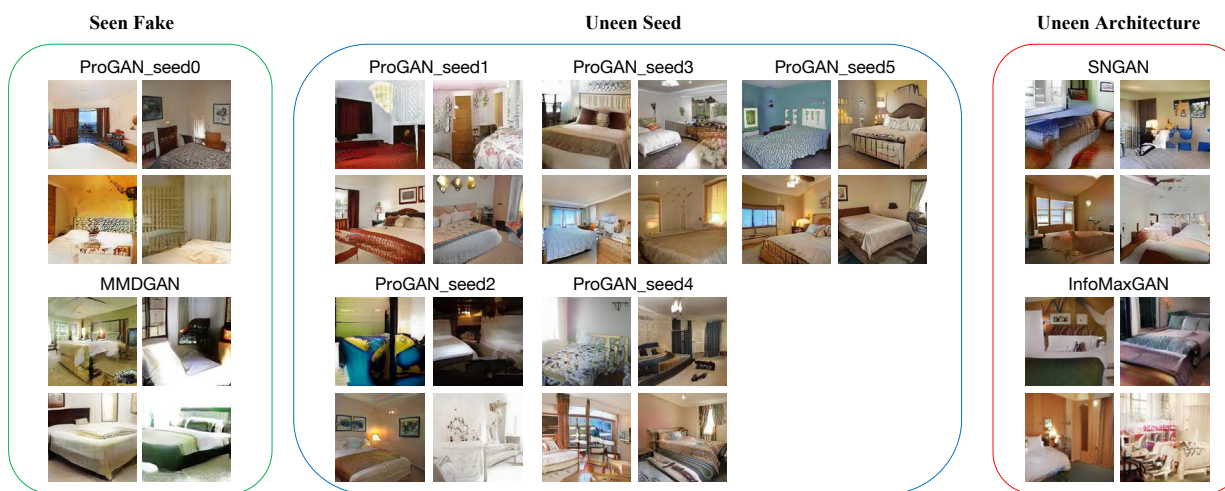


(a) CelebA



(b) Face-HQ

(c) ImageNet



(d) LSUN-Bedroom

Figure 12. Randomly selected samples for models trained on CelebA (a), Face-HQ (b), ImageNet (c), LSUN-Bedroom (d), LSUN-Cat (e), LSUN-Bus (f), and Youtube (g) dataset. Seen Fake, Unseen Seed and Unseen Architecture are based on Split 1 of the benchmark.

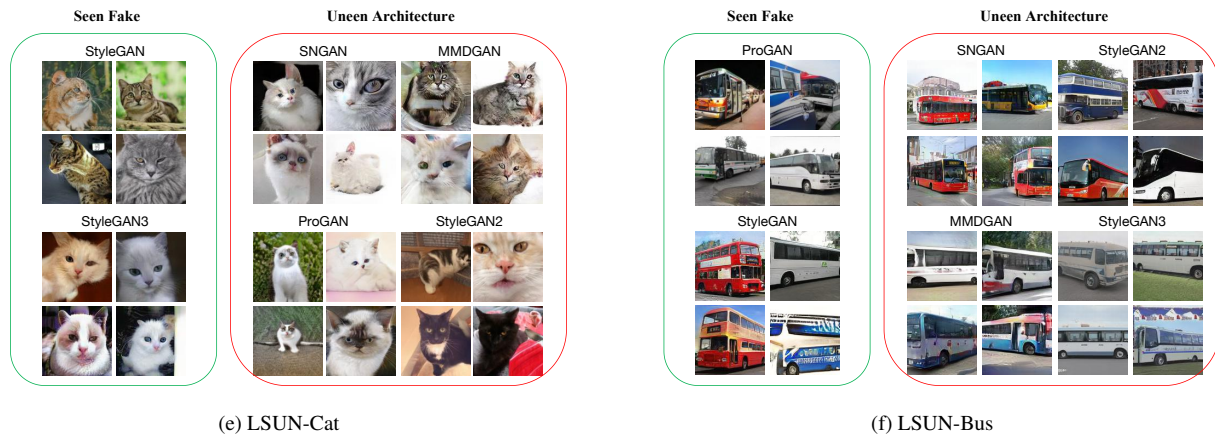


Figure 12. Randomly selected samples for models trained on CelebA (a), Face-HQ (b), ImageNet (c), LSUN-Bedroom (d), LSUN-Cat (e), LSUN-Bus (f), and Youtube (g) dataset. Seen Fake, Unseen Seed and Unseen Architecture are based on Split 1 of the benchmark. (cont.)